Online Supplement "Cardiac sarcomere length in situ and in vitro", Bub et. al

The software package and source code developed for semi-automated SL measurement is freely available. Please contact gil.bub@dpag.ox.ac.uk for details.

Supplement Section 1: Data analysis:

Off-line compensation for in-plane error: To correct for in-plane errors in path alignment perpendicular to striation patterns, and to account for measurement errors associated with artefacts associated with path length (resolution bias error), the program optionally iterates over a sequence of path angles (±5 degrees from the original path, 1 degree steps) and lengths (±10 pixels). For each angle the program averages the periods found for the range of ruler lengths, and determines the magnitude of the DFT peak. Angles where the DFT peak magnitude are less than that of the original are discarded, and the user path angle is reset so that the fluorescence intensity period is minimized. This method was found to converge to the correct periodicity within 0.2 % for a wide range computer generated striation patterns. We opt to report uncorrected data in the present publication since the algorithm may introduce a bias in the measurements. The computer generated striation patterns used to test the algorithm assume a perfectly periodic underlying SL pattern. The corrected trajectories may underestimate SL if there are significant sarcomere-to-sarcomere length variations within each cell.

Additional filtering criteria for SL measurements: In order to remove measurements biased by tissue motion or poor image quality, all measurements were filtered based on the relative magnitude of the peaks of the DFT obtained from the trajectories intensity profiles. Measurements were discarded if the magnitude of the highest DFT peak was less than 3 fold greater than any neighbouring peak corresponding to a SL period between 1.4 to 3.0 μm. Some data sets were also filtered based on experiment time (parsed from Leica meta-data files on an image by image basis) and ruler angle in the image plane as described in Results.

Operator bias: Each operator has to visually identify cells within each image that have clear striation patterns prior to drawing a path through the cell. Since the initial choice of cells is subjective, operators measure SL from different sub-populations of cells within the data sets. In addition, the location of the path within each cell is operator-dependent; parallel paths within a cell that give acceptable intensity profiles and sharp frequency peaks may give slightly different values for SL. In order to assess the effect of operator bias on the final measurements, four data sets were independently analysed by three different operators. Initial assessment of the three data sets revealed that one of the operators had drawn several trajectories that crossed cell boundaries and were outside the 5 degree range that could be compensated for by the off-line angle correction algorithm. The results from this operator had a significantly increased median SL value. The trajectories were re-drawn by the same operator using stricter guidelines. The resulting corrected mean SL and distribution *mode* fell within a 1% range of aggregate values.

Supplement Section 2: Monte Carlo estimation of error bounds on measurement:

Monte Carlo Estimates of SL distribution: In order to guide theoretical estimates of the lower bound of SL_R, we simulate the effect of cell angle on SL_M as a function of length of the cell in the imaging plane (L), prescribing a normal distribution of SL_R (mean 2.0 μm, variance

0.01), cell dimensions of l=142 μm, w=32 μm, h=13 μm (obtained from a widely referenced study by Satoh et al. (26)), and randomly chosen orientations relative to the image plane (see Methods). Figure S1 shows the probability distributions of SL_M for three different minima of user-defined path lengths (L_{min}) for SL_R with the above stated normal distribution (black continuous line). SL is well constrained for L_{min} = 90 μm and L_{min} = 70 μm, but is poorly constrained for L_{min} = 50 μm. However, it is evident from Figure S1a that the *mode* of the distribution while biased towards longer SL with reduced L_{min}, is relatively unaffected.

Figure S1b plots mean measured SL and the *mode* of the distributions of SL for L_{min} between 40 and 120 μm. Both the mean and *mode* overestimate the true mean of the underlying SL distribution, but the magnitude of the overestimate for the mean is far greater than that of the *mode*. This is particularly evident at shorter $L_{min.}$ Although the *mode* of the distribution is closer to the underlying SL than the measured mean, the accuracy of the *mode* estimate depends on the sample size. Figure S1c shows an error estimate for the *mode* calculation as a function of n, determined from the standard deviation of the *mode* estimates for multiple distributions of size n. The error associated with the *mode* estimate is high for small numbers of samples, but reaches less than 0.02 μm (1% of the base SL measurement) for n>150 samples.

The Monte-Carlo simulations do not allow one to directly calculate mean SL, because cell alignment relative to the imaging plane is not uniformly distributed in the real data (see Discussion). For this reason, we conducted simulations to estimate an upper and lower bound for the underlying mean of the distribution. A function of the magnitude of the estimates bounds can be obtained by first fitting an exponential to the results shown in figure S1b:

$$\text{Eq. 1} \quad F(L_{min}) = 0.0599\, \mathbf{e}^{-0.0177 L_{min}} + 1.0$$

Similarly, the error in estimating the *mode* of the distribution is given by a fit to the simulation results shown in figure S1c:

$$\text{Eq. 2} \quad G(n) = 0.0479\, \mathbf{e}^{-0.0198 n} + 0.016$$

where n is the number of samples in the data set with $L \geq L_{min}$. The 'true' mean SL is expected to lie between an upper bound (*mode* + G(N)) and a lower bound (*mode*-F(L_{min}) -G(n)).The magnitude of the bounds is therefore given by:

$$\text{Eq. 3} \quad H(L_{min}, n) = F(L_{min}) + 2\, G(n)$$

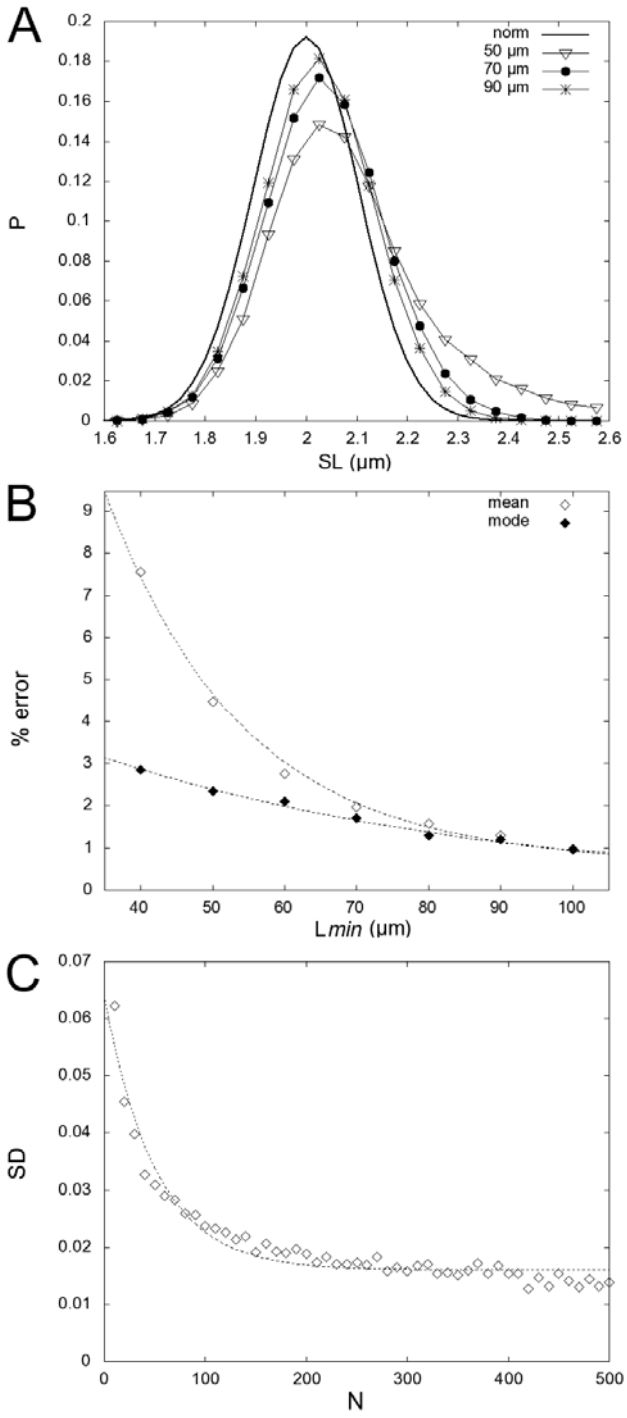

FIGURE S1. Monte-Carlo simulations of the effect of cell angle on SL_M. A) Simulations, assuming a completely random cell orientation relative to the image plane, shift and skew a normally distributed SL distribution (dark line) as a function of minimum length of the analysis path(L_{min}) in the image plane (diamonds: L_{min}= 50 µm , circles: L_{min}= 70 µm, stars: L_{min} = 90 µm). B) SL_M overestimation error as a function L_{min}. Open diamonds show percent increase in measured *vs*. actual mean; closed diamonds illustrate percent increase in measured vs actual *mode*. The distributions *mode* is determined by kernel density estimation as described in the text C) Standard deviation (SD) of the mode estimate as a function of the number of samples in the distribution. Dashed lines in panels B and C are exponential

functions fitted to the simulation results, using a non-linear least-squares (NLLS) Marquardt-Levenberg algorithm (Gnuplot, www.gnuplot.org).

Section 3: Compensation for tissue motion:

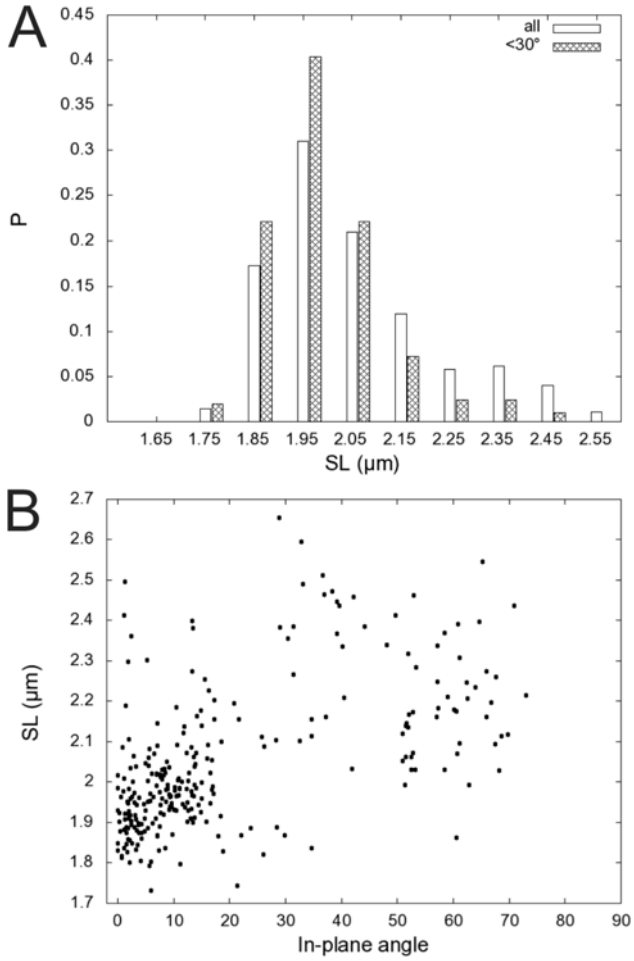

FIGURE S2. A: Distribution of sarcomere lengths measured from the intact Langendorff-perfused rat heart. Open bars: SL for all cells; Hatched bars: cells aligned within 30 degrees of the fast scan axis of the two photon fluorescence microscope. B: SL as a function of cell orientation in the image plane (cells at 0 degrees are aligned in parallel with the fast scan axis of the two photon fluorescence microscope).

Mean SL from the first 5 minutes of recording time (i.e. about 30 minutes after sacrifice) was 2.05±0.18 μm (n = 300; N = 11 experiments). Means in individual experiments varied from 1.89±0.06μm to 2.36±0.10 μm. A histogram (Fig S2a, open bars) of SL_M shows a dominant peak in SL frequency between 1.9 and 2.0 μm, and a second lower peak between 2.3 and 2.4 μm. The second peak is predominantly comprised of SL measurements from 2 experiments, although infrequently cells with long SL were observed in most experimental runs. Although we do not rule out that a population of long SL cells exists in our preparation, further analysis suggests that the second peak is caused by an experimental artefact, as described next.

Figure S2b shows the dependence of measured SL and angle between the cell's long axis and

the imaging plane x-axis (corresponding to the fast scan axis of the microscope). Cells aligned with the x-axis display shorter SL_M and less variance than cells at other angles. We hypothesize that the in-plane angle dependence on SL is caused by the interplay of tissue motion (unavoidable in Langendorff perfused living tissue), local cell length changes, the large difference in acquisition times for a single scan line (~3ms) and a whole frame (1,625 ms), and the scanning direction of the two photon microscope excitation light. If we filter the data set by excluding SL measures that fall outside of ±30º of the fast scan axis of the microscope, we obtain a mean SL of 1.99± 0.12 μm. The histogram of filtered SL has a unimodal distribution (Figure 7a, hatched bars) with a peak between 1.9 and 2.0 μm.

The presence of a correlation between in-plane imaging angle and SL_M supports the hypothesis that non-structural aspects, such as tissue motion, modulate SL_M in the intact isolated heart. Two-dimensional images are built up from a series of sequentially acquired data points, resulting in data being rapidly collected for cells aligned along the x axis of an image (3 ms), and two orders of magnitude more slowly (1.625 s) for cells aligned along the y-axis of the image. Tissue drift can both increase and decrease SL_M, however we observe an increase in SL_M with cell angle. We believe that this bias may caused by two mechanisms.

First, compression due to motion distortion may reduce SL contrast. Since operators tend to favour images of cells with clear, well separated striation patterns to define long analysis paths, cells with short SL may be under-sampled in images with both motion-induced reduction and enhancement of apparent SL.

Alternatively, motion may be caused by transient sporadic cell contractions, as opposed to bulk movement of the entire tissue. Although the arrested tissue is largely quiescent, intermittent local contractions are nonetheless expected to occur. These regional transient contraction events would stretch cells in the surrounding tissue volume. Assuming that the area in which stretched tissue may be found is greater than that occupied by the contracting cell population, and taking into account the small imaging field of view, SL measurements are more likely to cell stretch rather than contraction.

Both the tissue drift and local tissue contraction mechanisms suggested above are speculative, and at present we do not have a method for confirming or refuting either of them. It is clear, however, that experimental procedures may be optimized by using the fast scan direction of the microscope as a guide for cell alignment before acquisition of images.